ACI TECHNICAL SESSION - MARCH 26, 2001

NONDESTRUCTIVE EVALUATION OF CONCRETING PROBLEMS IN SOME LARGE-VOLUME STRUCTURES

Allen G. Davis and Malcolm K. Lim[1]

ABSTRACT

Problems during concreting of large mass structures do occur, such as segregation, localized poor concrete consolidation or cracking caused by plastic or thermal shrinkage. Because of the volume of concrete concerned, it is often very difficult to develop an evaluation program that will fully measure the extent of any such problem. This paper describes case histories where nondestructive test methods have been used to minimize the amount of intrusive investigation needed to reach a sound engineering conclusion. The different test methods used in these cases will be reviewed.

INTRODUCTION

Hardened concrete properties of large mass concrete structures are difficult to evaluate because of the problem of scale. Invasive testing such as coring is limited for practical and economical reasons, and information obtained is restricted to a very small percentage of the total concrete volume. Also, surface features and anomalies do not necessarily reflect the internal concrete condition. These problems apply to the inspection of recently poured concrete structures and to the evaluation of existing structures in service.

Nondestructive testing (NDT) can contribute to an understanding of structural and material condition in large-volume structures. However, for the NDT program to be technically and cost beneficial, it must reduce the time and effort (and hence cost) spent in coring and laboratory testing, and at the same time present a technically accurate, broader view of the structure condition. If these criteria cannot be met, then the Engineer will not benefit from and should not rely on NDT.

NDT methods such as traditional ultrasonic pulse velocity (UPV), impact-echo, rebound hammer, infrared thermography and other relatively superficial tests are often unsuccessful in providing information about the concrete quality in the body of the structure, particularly when surface breakdown is present such as freeze-thaw damage and alkali aggregate reaction. This paper presents recent case histories where three NDT techniques were valuable in evaluating and quantifying problems within large concrete volumes:

- Impulse Response (IR)
- Spectral Analysis of Surface Waves (SASW)
- Impulse Radar.

---

[1] Senior Principal Engineer and Senior Engineer, Nondestructive Evaluation, Construction Technology Laboratories (CTL) Inc., Skokie, Illinois, USA

velocity spectrum is divided by the force spectrum to obtain a transfer function, referred to as the *Mobility* of the element under test. The test graph of Mobility plotted against frequency over the 0-1kHz range contains information on the condition and the integrity of the concrete in the tested elements, obtained from the following measured parameters:

- *Dynamic Stiffness:* The slope of the portion of the Mobility plot below 0.1 kHz defines the compliance or flexibility of the area around the test point for a normalized force input. The inverse of the compliance is the dynamic stiffness of the structural element at the test point. This can be expressed as:

  Stiffness f *[concrete quality, element thickness, element support condition]*

- *Mobility and Damping:* The test element's response to the impact-generated elastic wave will be damped by the element's intrinsic rigidity (body damping). The mean mobility value over the 0.1-1 kHz range is directly related to the density and the thickness of a plate element, for example. A reduction in plate thickness corresponds to an increase in mean mobility. As an example, when total debonding of an upper layer is present, the mean mobility reflects the thickness of the upper, debonded layer (in other words, the slab becomes more mobile). Also, any cracking or honeycombing in the concrete will reduce the damping and hence the stability of the mobility plots over the tested frequency range.

- *Peak/Mean Mobility Ratio:* When debonding or delamination is present within a structural element, or when there is loss of support beneath a concrete slab on grade, the response behavior of the uppermost layer controls the IR result. In addition to the increase in mean mobility between 0.1 and 1 kHz, the dynamic stiffness decreases greatly. The peak mobility below 0.1 kHz becomes appreciably higher than the mean mobility from 0.1-1 kHz. The ratio of this peak to mean mobility is an indicator of the presence and degree of either debonding within the element or voiding/loss of support beneath a slab on grade.

SPECTRAL ANALYSIS OF SURFACE WAVES (SASW)

This nondestructive, stress wave test was developed for concrete highway and airport pavements, and uses surface waves to determine the thickness and elastic properties of different slab layers. Nazarian *et al* [9] adapted the technique to establish the relationship between wavelength and velocity for these surface waves by digital signal processing, and the method has been extended to assess concrete damage within slabs and beams [10].

The surface, or R-wave generated in this test contains a range of components of different frequencies or wavelengths. (The product of frequency and wavelength equals wave speed). This range depends on the contact time of the impact; a shorter contact time results in a broader range. The longer wavelength (lower frequency) components penetrate more deeply, and this is the key to using the R-wave to gain information about the properties of the deeper layers. In a layered

system, such as a non-cracked layer above a cracked layer, the propagation speed of these different components is affected by the wave speed in those layers through which the components propagate. A layered system is a dispersive medium for R-waves, which means that the different frequency components of the R-wave propagate with different speeds, which are called phase velocities.

Phase velocities are calculated by determining the time it takes for each frequency (or wavelength) component to travel between two receivers. These travel times are determined from the phase difference of the frequency components arriving at the receivers. The phase differences are obtained by computing the cross-power spectrum of the signals recorded by the two receivers. The phase portion of the cross-power spectrum gives phase differences (in degrees) as a function of frequency. The phase velocities are determined as follows:

$$C_{R(f)} = X(360/\Phi_f).f$$

where $C_{R(f)}$ = surface wave speed of component with frequency f,
X = distance between receivers,
Φ_f = phase angle of component with frequency f.

The wavelength λ_f corresponding to a component frequency, f is calculated using the following equation:

$$\lambda_f = X(360/\Phi_f)$$

By repeating the calculations in these two equations for each component frequency, a plot of phase velocity versus wavelength is obtained. Such a plot is called a dispersion curve.

A process called inversion is then used to obtain the approximate stiffness profile at the test site from the experimental dispersion curve. (As an example, a horizontal layer with a vertical crack will appear much less stiff than a continuous layer). The test site is modeled as layers of varying thickness. Each layer is assigned density and elastic constants. Using this information, the solution for surface wave propagation in a layered system is obtained and a theoretical dispersion curve is calculated for the assumed layered system. The theoretical curve is compared with the experimental dispersion curve. If the curves match, the problem is solved and the assumed stiffness profile is correct. If there are significant discrepancies, the assumed layer system is changed, or refined and a new theoretical curve is calculated. This process is continued until there is good agreement between the theoretical and experimental curves.

IMPULSE RADAR TEST METHOD

The impulse radar technique is based on principles of electromagnetic wave reflection. The radar system radiates short time-duration electromagnetic pulses (0.5 to 1.5 nanoseconds) into the material to be examined from a broadband antenna, which is electromagnetic ally coupled to the material's surface [11]. The antenna houses the transmitter as well as the receiver. For most concrete testing applications, a contact transducer the size of a hand-held calculator is passed over the surface to be tested, transmitting an electromagnetic wave into the structure. When the electromagnetic wave travels through different media with different dielectric constants a portion of the wave is reflected back to the antenna and the remainder of the wave is refracted into the next medium. Reflected pulses are received by the transducer and electronically processed. New

technology has made coloring capability of the output possible in addition to numerous functions such as filtering and arithmetic summation. The loss of strength of the reflected waveform, measured in volts, is used in data evaluation. When voids are met, these pulses are reflected by the difference in the dielectric constants of the concrete and the air in the void.

Impulse radar has a wide range of applications in testing concrete, such as detection of delaminations, voids and dowel bar alignment. The technique also shows potential for other applications such as monitoring cement hydration or strength development in concrete, studying the effect of various admixtures on concrete curing, determination of water content in fresh concrete, and measurement of concrete member thickness [12]. The moisture present and the amount and type of reinforcement influence the radar wave depth of penetration. Concrete as thin as 30 to 60 mm can be examined with high resolution or short pulse width (<1 ns) radar antennas. For dry and unreinforced concrete, radar can penetrate to depths of approximately 0.6 m to detect the location and depth of defects.

CASE HISTORIES

Mine Shaft Plug

The mass concrete plug fills the original rock tunnel, and is approximately 2.7 m wide by 3.6 m high at the visible face, and approximately 4.5 m deep. The rock surrounding the plug appears to be hard and compact at the plug face. Water seepage is visible at the top face, and it is not clear whether this seepage is coming from the rock or from the concrete/rock interface, or both. Figure 1 shows the downstream plug face. Two drain outlet valves are visible on the plug face: at approximately 1 m from the left and right edges respectively and approximately 1m from the base of the plug. In addition, a sealed pipe is apparent in the top right corner, which is thought to be the entry point of the original concrete tremie. The sheen on the concrete face is from the water seepage. Several 25 mm-diameter grout pipes are also notable at the top right corner of the plug.

The plug was tested using the IR method, and two testing approaches were adopted:

- A matrix of test points at 600-mm vertical and horizontal spacing was established on the plug face, and each test point was impacted with the geophone located at approximately 150 mm from the point of impact. This test methodology gives information on the concrete condition to a depth of approximately 900 mm into the plug from its face, as described above. This was entitled *IR – Concrete Quality*.
- The geophone was positioned at the center of the plug face, and each test was performed by striking the face at points around the periphery of the plug. A digital gain of either 10 or 20 was applied to the velocity response from the geophone to amplify the signal strength, in view of the damping effect of the seated plug. The test data that can be interpreted using simulation methods originally developed for testing the length and integrity of drilled shafts and caissons such as the Impedance Log. and

the test method is fully described in the Appendix to this paper. This was entitled *IR – Plug/Rock Interface.*

IR – Concrete Quality: The 600-mm x 600-mm test grid laid out over the total plug face gave a grid with 5 test points from left to right in the horizontal direction (Columns A to E) and 6 test points from bottom to top (Rows 1 to 6). The measured values of dynamic stiffness and average mobility are plotted in contour form in Figures 2 and 3 respectively, and show that the values of stiffness and average mobility are relatively consistent over most of the plug face, apart from a zone around column D, from test rows 3 to 6. It is expected that the average mobility will decrease from the center of the plug to the edge, and that the inverse will happen for the measured stiffness. This is the case for three of the four plug face quadrants (SE, SW and NW), whereas the fourth quadrant shows considerably higher values for average mobility and correspondingly much lower values of stiffness.

It is of interest to note that these poorer results come from a zone immediately surrounding and below the location of the original concrete tremie. The very high mobility values indicate that poor concrete consolidation is present in a zone approximately 1.2 m high by 600 mm wide at the locations shown in the northeast quadrant.

IR – Plug/Rock Interface: The Impulse Response results obtained in this mode were analyzed to measure the distance from the face to the back of the plug and the equivalent dynamic shear modulus at the concrete rock interface at different points around the plug.

Typical values for concrete stress wave velocities in integral foundation piers with good concrete quality vary between 3,800 and 4,200 m/s, with average values around 4,000 m/s. The depth of the plug measured with the mobility plots assuming a stress wave velocity in the concrete of 4,000 m/s varied between 4.4 m and 4.7 m (See Figure 4). If the projected plug depth of 4.57 m is substituted, then the concrete stress wave velocity is between 3,870 and 4,130 m/s, indicating that the concrete in the plug is of good quality.

It was also possible to match the real mobility responses for the plug with a simulated response, as described in the Appendix. A simulated mobility plot is compared with an actual test result in Figure 5. The matching value for the shear wave velocity, ß at the concrete/rock interface is then obtained from the parameters used in the simulation model [3]. Values for the shear wave velocity at the rock/concrete interface for different points around the plug perimeter are presented in Table 1 below.

As a comparison, measured values for ß for rock-socketed caissons are usually in the range of 300 to 400 m/s for strong concrete/rock bond. The very high values measured here indicate a very good bond between the concrete and the rock.

Lower values for ß (between 450 and 500 m/s) are concentrated around the bottom center and the top of the plug, with high values along the sides of the plug over the lower two thirds. This is to be expected, as a result of the concrete placement technique employed.

Table 1

Test Location (Column-Row)	Shear Wave Velocity, ß (m/s)
A-2	750
A-3	750
A-5	500
B-2	750
C-1	450
C-6	450
D-2	500
D-5	600
D-6	450
E-1	750
E-2	750
E-3	750
E-5	450

Thick Foundation Raft

This basement concrete raft has a nominal thickness of 1.8 m with thickening at column bases to approximately 2.5 m. Design drawings indicate that the slab is reinforced at the top and the bottom, with extra reinforcing dowel bars at half slab thickness at construction joints. Typical slab construction joints are located at halfway between column lines, and drawings show each joint has a water stop above and below the central dowel bar. Generally, these joints are not visible since the slab is covered by a surface coating approximately 25 mm thick. No cracks are presently visible through the coating layer, which was applied approximately 8 years ago. Deflections in this slab have been monitored since the start of construction of a nearby tunnel. Deflection changes at locations along three column lines could be interpreted as onset of cracking in the basement slab. Vertical changes at displacement monitoring points (DMP) on the floor suggest that cracking may have occurred at three locations.

The overall contour plots established from DMP readings for differential slab vertical displacements show depressions forming at two of these three locations, suggesting that any cracking in the slab would be more apparent in the bottom third of the slab thickness. In order to locate possible cracking at that depth in the slab, a combination of two stress wave methods was proposed:

- The Impulse Response (IR) method
- The Spectral Analysis of Surface Waves (SASW).

In this investigation, the IR test was used to:

- Locate the presence of any near-vertical cracks in the slab, by observing changes in stiffness and mobility either side of the crack,
- Measure the approximate thickness of the floor slab at specific points.

IR test results close to discontinuities such as vertical joints or cracks always show an increase in average mobility and a reduction in stiffness. If the slabs on either side of the joint or crack are independent of one another, there is usually a noticeable difference in both parameters measured on either side. If a good mechanical connection or stress transfer exists across the joint or crack between the two slabs (such as dowel bars and other stress transfer mechanisms), the stiffness on either side of the discontinuity are similar.

The SASW test was used in this investigation to locate any open vertical or near-vertical cracks in the floor slab, and to measure their approximate depth. Five principal SASW test lines were set up, with parallel test lines in some cases. Each test comprised placing the two accelerometers at a fixed distance apart (in this case, either 0.9 m or 1.8 m was chosen as the increment), and an impact generated in line with the accelerometers. The aggregate time taken for the surface wave to travel between the two accelerometers was recorded for each test. Knowing the distance between the accelerometers, the apparent surface wave speed can be measured. Normally, for good concrete the surface wave speed is between 1,980 m/s and 2,280 m/s.

Additionally, the reduction in signal strength from the accelerometer nearer the impact source to that further away can be measured. This is referred to as the surface wave damping ratio. For normal concrete over an accelerometer spacing of 1.8 m, this damping ratio is less than 10. If a significant increase in damping ratio is recorded, together with a decrease in apparent surface wave speed, a vertical barrier such as a crack or joint is located between the two accelerometers. The degree of severity or "openness" of the crack is indicated by the amount of the reduction in surface wave speed and the increase in the damping ratio.

When a potential vertical crack/joint is located in this manner, the surface wave speed and the surface wavelength can be calculated as a function of the frequency spectrum, as in the method description above. In continuous layered media, the values of surface wave speed increase relatively linearly with increasing frequency. However, when discontinuities are present, the surface wave speed reaches a maximum value at a relatively low frequency, and remains constant or decreases above that frequency.

Profiles of the slab average mobility and stiffness gave relatively uniform mobility and stiffness values. Average mobility is usually between 1.5 and 2.5, and stiffness generally is greater than 1.5 MN/mm. These are the values normally associated with slabs of this thickness. Exceptions were noted, as shown in Figure 6, where a relatively high mobility and low stiffness at test point #11 probably corresponded to a debonding of the coating immediately over a construction joint. There are no signs of any slab distress at the surface. As a result of these test results, SASW profiles were selected across potential vertical slab separations.

Figures 7 and 8 show results obtained for apparent surface wave speed and damping ratio for two test locations along one profile. Figure 7 shows a normal damping ratio for continuous concrete of 4.48, together with a speed of 2,090 m/s. However, the test point in Figure 8 has a

$$k_b = 1.84\ r\ [\ E_b / (1-\nu_b{}^2)] \qquad (2)$$

where: r is the shaft radius,

E_b and ν_b are the Young's modulus and Poisson's ratio for the soil at the base.

For each of the shaft segments from the top downwards, the following parameters are calculated cumulatively:

- Body and soil damping coefficient, σ; [5,6,7]
- Segment impedance, taking into account the geometric and damping properties;
- Variation of impedance with frequency (from $\coth(\sigma l)/\tanh(\sigma l)$). [5,6,7]

At the bottom of each segment, the effect of its impedance is added to the impedance from the previous calculations, in the form of a complex array representing the variation of impedance with frequency. The inverse of the magnitude of the complex entry of this array when summed at the end of the cumulative calculation is the simulated mobility for the pile as a function of frequency. By remaining in the frequency mode, magnitudes of force and velocity do not have to be known or assumed for simulation. In this way, changes in shaft and soil properties can be assigned to successive shaft segments. The relatively large number of variables means that several simulation solutions are available. In particular, the selection of the β value is important. This value can range between 50 m/s (soft clays) to over 300 m/s (rock sockets). Figure 2 is an example of an idealized simulation response.

REFERENCES

1. American Concrete Institute Report ACI 228.2R-98, "*Nondestructive Test Methods for Evaluation of Concrete in Structures*". ACI, Farmington Hills, Michigan, 62 pp.
2. Sansalone, M. and W.B. Streett, 1997, "Impact-Echo: Nondestructive Evaluation of Concrete and Masonry," Bullbrier Press, Ithaca, NY, 339 pp.
3. Davis, A. G. and C.S. Dunn, "From Theory to Field Experience with the Nondestructive Vibration Testing of Piles," *Proc. Instn Civ. Engnrs*, Part 2, 1974, 57, Dec., 571-593.
4. Davis A.G. and B.H. Hertlein 1987, "Nondestructive testing of concrete pavement slabs and floors with the transient dynamic response method," *Proc. Int. Conf. Structural Faults and Repair*, London, July 1987, Vol. 2, pp. 429-433.
5. Davis, A.G. and B.H. Hertlein, 1995, "Nondestructive testing of concrete chimneys and other structures," *Conf. Nondestructive Evaluation of Aging Structures and Dams*, Proc. SPIE 2457, 129-136, Oakland CA, June 1995.
6. Davis, A.G., J. G. Evans and B.H. Hertlein, 1997, "Nondestructive evaluation of concrete radioactive waste tanks," *Journal of Performance of Constructed Facilities*, ASCE, Vol. 11, No. 4, November 1997, pp. 161-167.
7. Davis, A.G. and J. Kennedy, 1998, "Impulse Response testing to evaluate the degree of alkali-aggregate reaction in concrete drilled-shaft foundations for electricity transmission towers", *Conf. Nondestructive Evaluation of Utilities and Pipelines II*, Proc. SPIE 3398, 178-185, San Antonio, TX, April 1998.

8. Davis, A.G., B.H. Hertlein, M. Lim and K. Michols, 1996, "Impact-Echo and Impulse Response stress wave methods: advantages and limitations for the evaluation of highway pavement concrete overlays," *Conf. Nondestructive Evaluation of Bridges and Highways*, Proc. SPIE 2946, 88-96, Scottsdale AZ, December 1996.
9. Nazarian, S., K.H. Stokoe II and W.R. Hudson, 1983, "Use of Spectral Analysis of Surface Waves Method for Determination of Moduli and Thickness of Pavement Systems", *Transportation Research Record,* No. 930, Transportation Research Board, Washington, D.C., pp. 38-45.
10. Kalinski, M.E., K.H. Stokoe II, J.O. Jirsa and J.M. Roesset, 1994, "Nondestructive Evaluation of Internally Damaged Areas of a Concrete Beam using the SASW Method", *Preprint 9407114,* Transportation Research Board 73rd Annual Meeting, Washington, D.C., January 1994.
11. "Detection of Delamination and Cavities in Concrete," Maryland Department of Transportation, FHWA/MD-87/05, August 1986.
12. G. G. Clemeña, 1991. "Short-Pulse Radar Methods," Chapter 11 in *Handbook on Nondestructive Testing of Concrete*, CRC Press, Boca Raton, FL.

Average Mobility

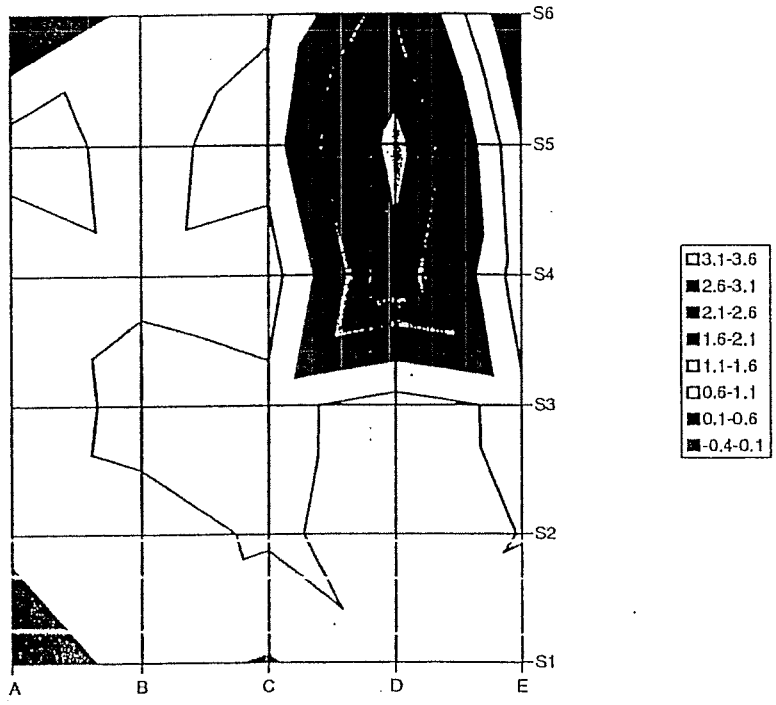

Stiffness (MN/mm)

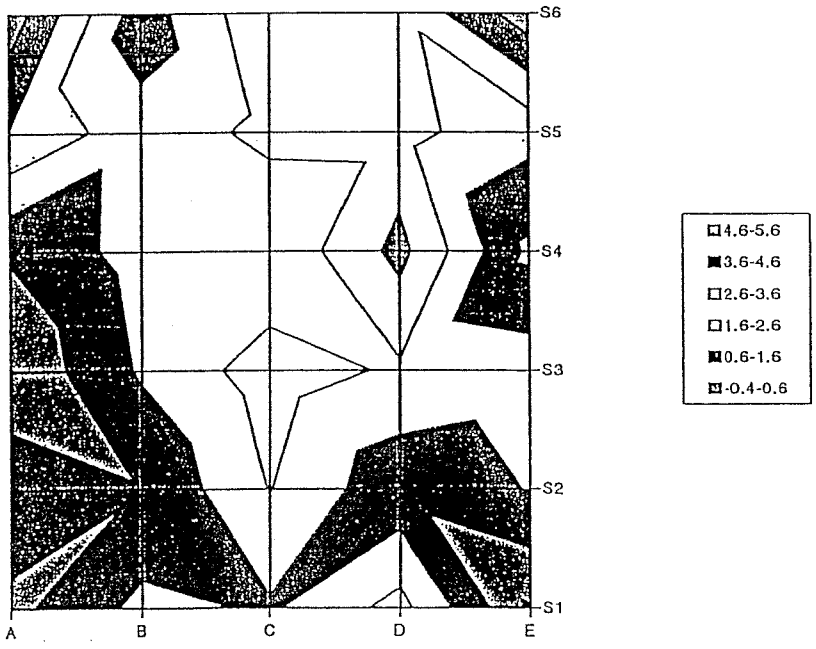

Figures 2 & 3. Mine Plug Average Mobility and Stiffness Contours

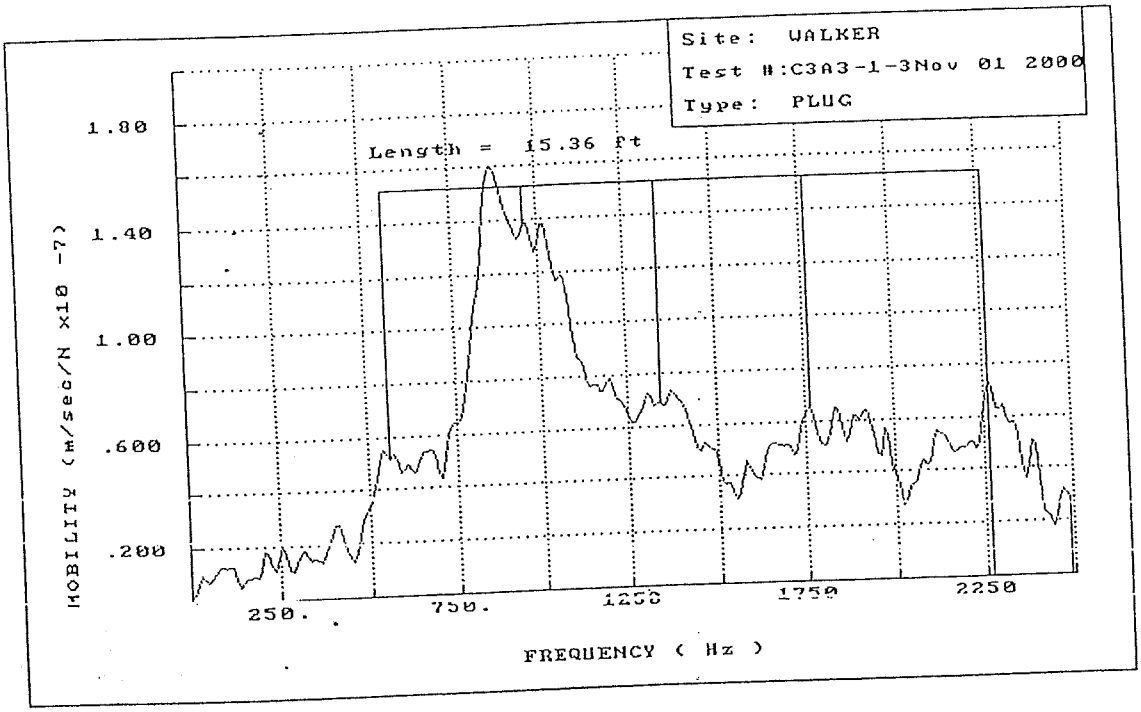

Figure 4. IR test response – Plug Depth Measurement

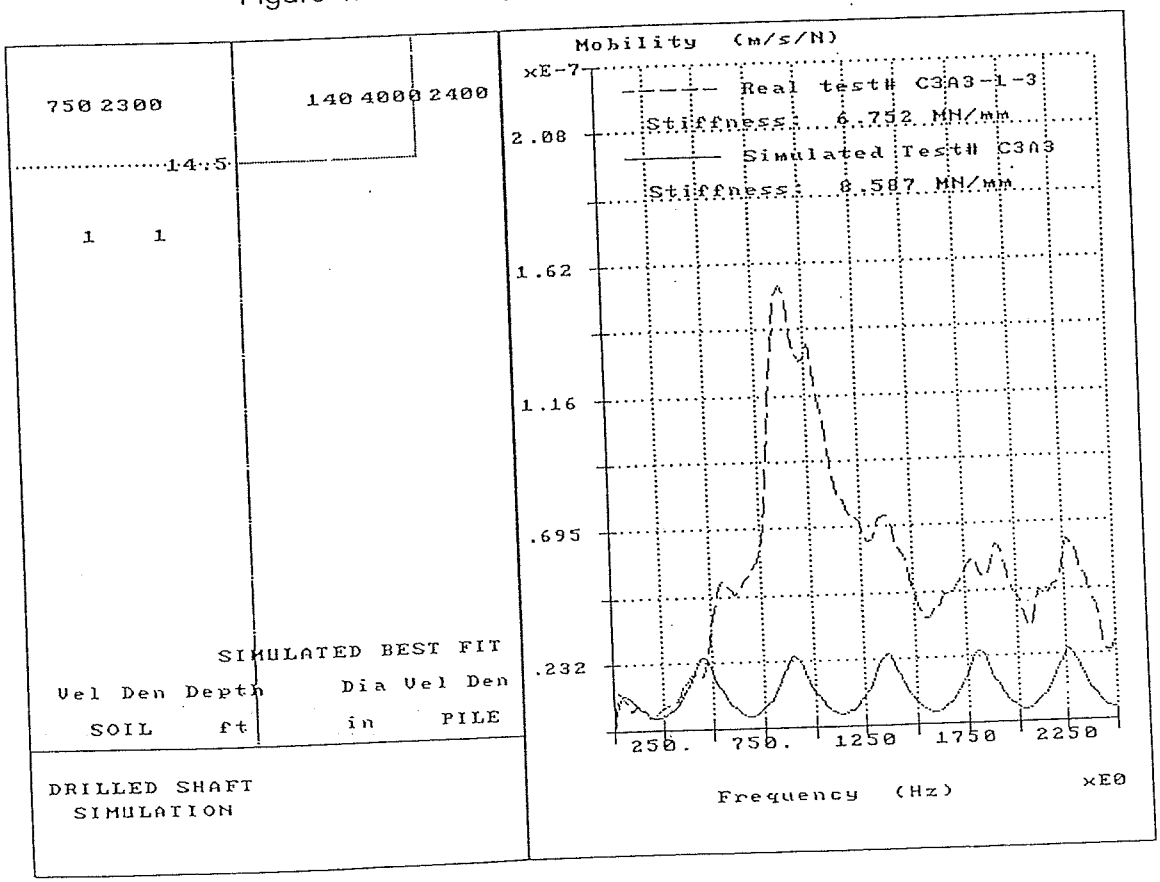

Figure 5. Simulation Plot of Mine Plug IR Response

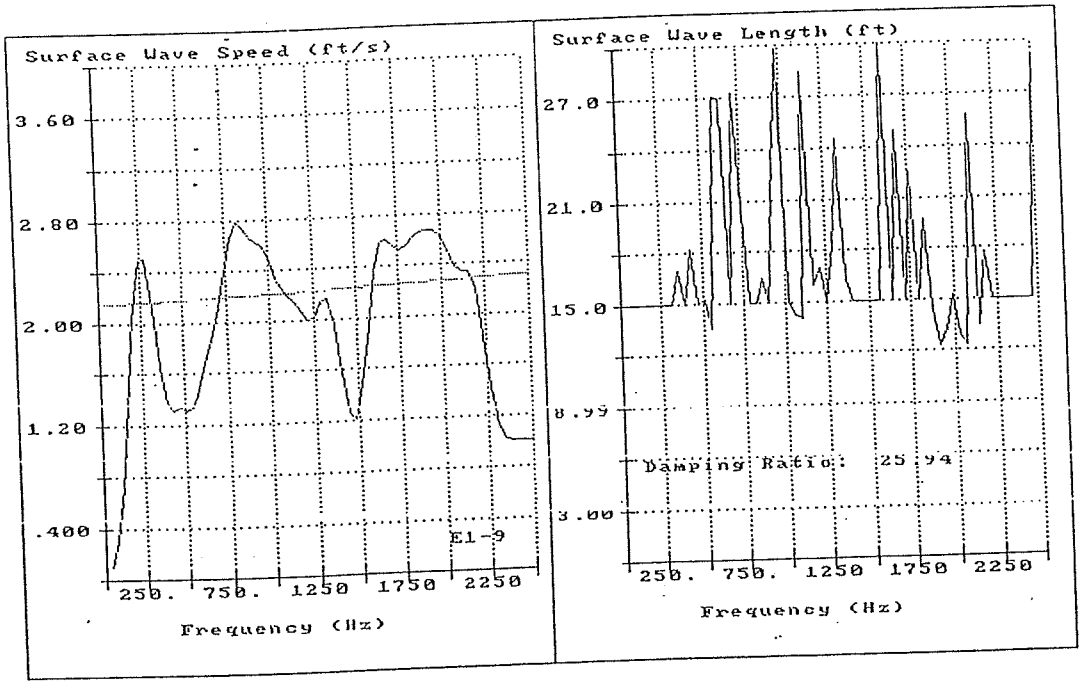

Figure 8. SASW Surface Speed v. Frequency – Vertical Crack in Concrete Slab

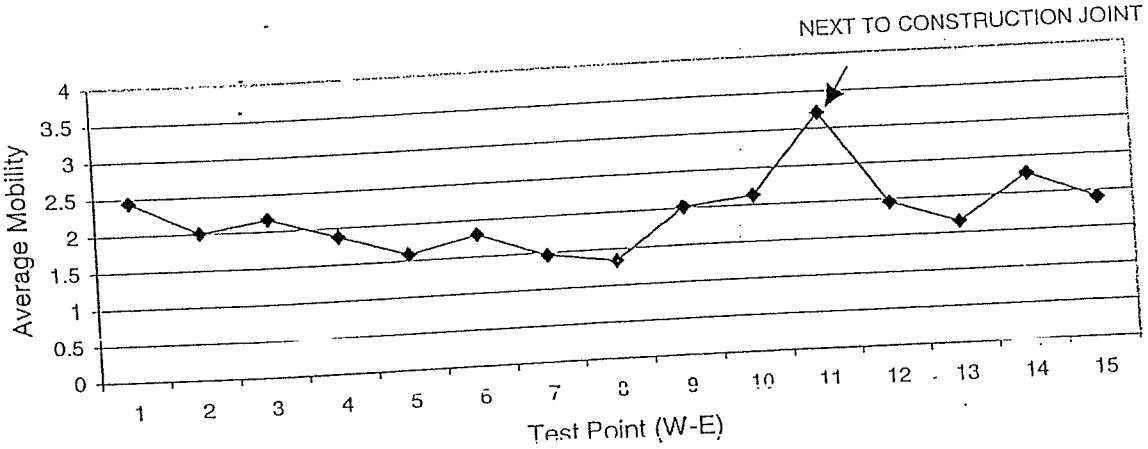

Figure 6. Impulse Response profile along basement slab

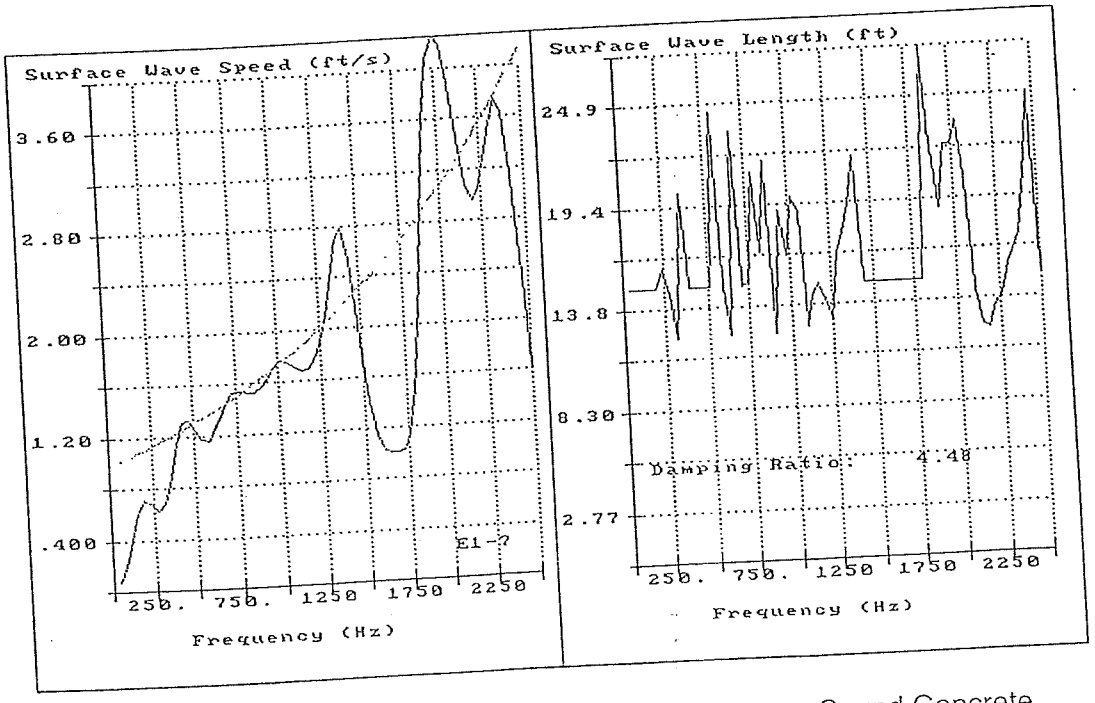

Figure 7. SASW Surface Speed v. Frequency – Sound Concrete

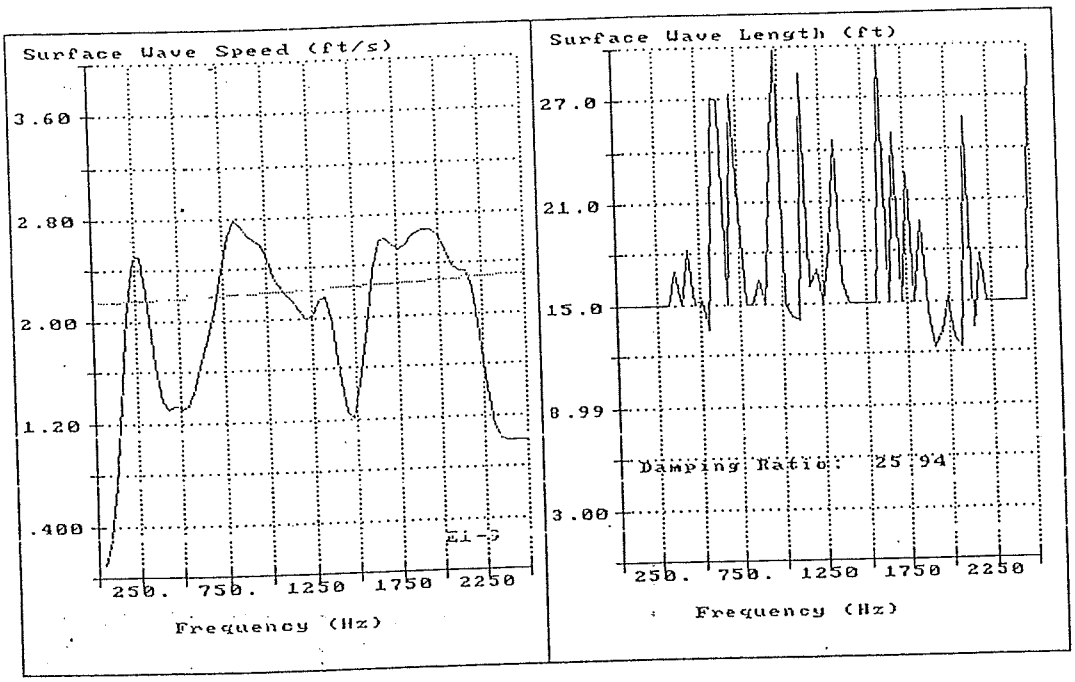

Figure 8. SASW Surface Speed v. Frequency – Vertical Crack in Concrete Slab